

Supplementary Information

Rapid Collagen Directed Mineralization of Calcium Fluoride

Nanocrystals with Periodically Patterned Nanostructure

Wei-jian Fang¹, Hang Ping^{1}, Wolfgang Wagermaier², Shen-bao Jin³, Shahrouz Amini², Peter Fratzl², Gang Sha³, Fan-jie Xia¹, Jin-song Wu¹, Hao Xie⁴, Peng-cheng Zhai¹, Wei-min Wang¹, and Zheng-yi Fu^{1*}*

¹State Key Laboratory of Advanced Technology for Materials Synthesis and Processing, Wuhan University of Technology, Luoshi Road No. 122, Wuhan, 430070, China.

²Department of Biomaterials, Max Planck Institute of Colloids and Interfaces, Am Mühlenberg 1, 14476 Potsdam, Germany.

³School of Materials Science and Engineering, Herbert Gleiter Institute of Nanoscience, Nanjing University of Science and Technology, Nanjing 210094, China.

⁴School of Chemistry, Chemical Engineering, and Life Science, Wuhan University of Technology, Wuhan 430070, China.

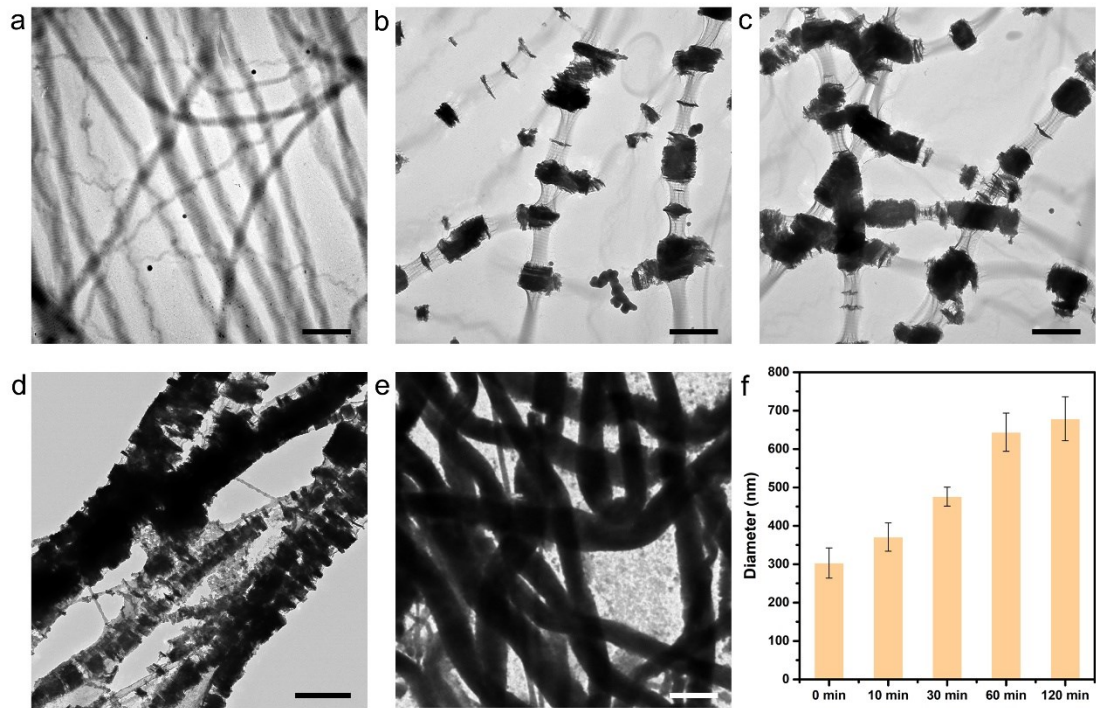


Figure S1. The low magnification of evolution processes of mineralized collagen fibrils. (a) Original collagen fibril, (b) mineralization for 10 min, (c) mineralization for 30 min, (d) mineralization for 60 min, (e) mineralization for 120 min. (f) Diameters of collagen fibrils at different time point during mineralization. (Scale bar in (a-e), 1 μm)

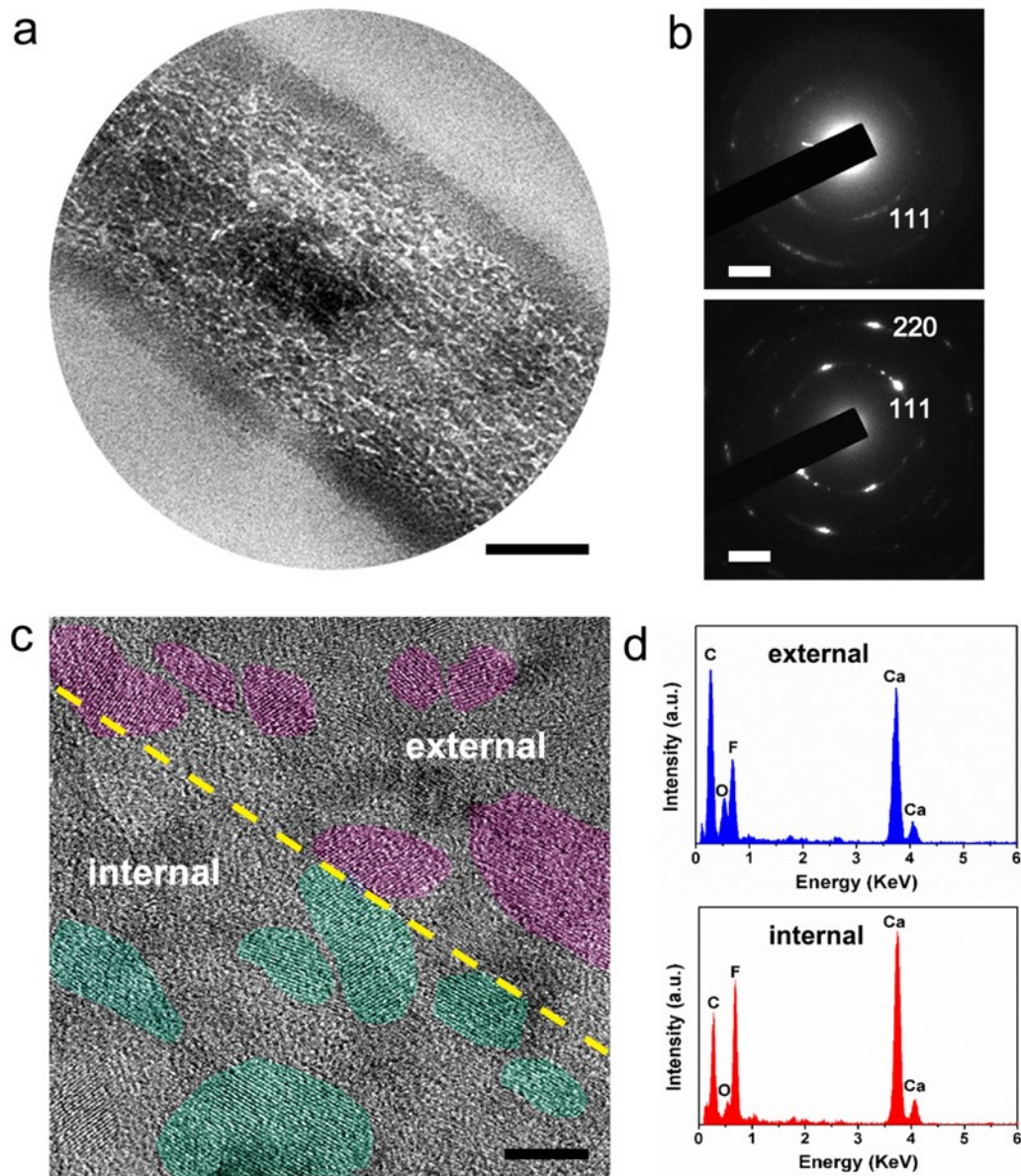


Figure S2. Structure of minerals in external and internal regions. (a) High magnification of longitudinal section TEM image (scale bar, 100 nm). (b) SAED patterns in external (upper) and internal (lower) regions (scale bar, 2 1/nm). (c) HRTEM image of interface between external and internal regions (scale bar, 10 nm). The lattice fringes were marked by red (external) and blue (internal), respectively. (d) EDS images of external (upper) and internal (lower) region. The content of calcium and fluoride elements in the internal region were higher those of the external region, indicated the high content of minerals deposited in the inner space of collagen fibrils.

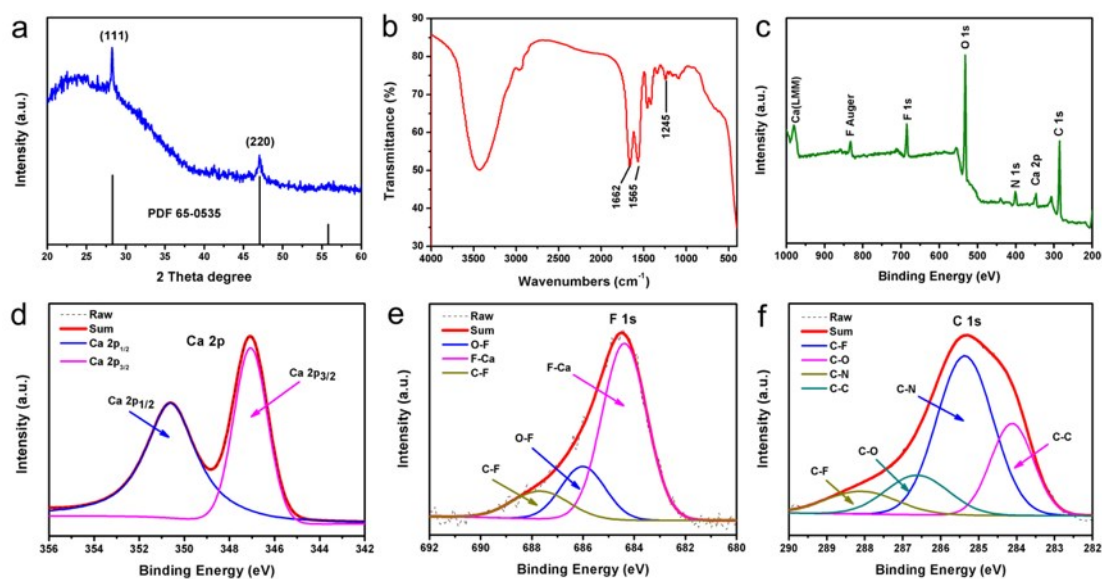


Figure S3. Phase and composition of mineralized collagen fibrils. (a) X-ray diffraction of the crystalline CaF_2 phases. (b) Fourier transform infrared reflection results of organic components. (c) X-ray photoelectron spectroscopy survey spectrum of elements corresponding to the organic and inorganic components. (d-f) High resolution deconvoluted spectrum of Ca 2p, F 1s and C 1s, respectively. The four deconvoluted peaks at 284.1, 285.4, 286.6, and 288.1 eV in the C 1s spectrum are ascribed to C–C, C–N, C–O and C–F bonds, respectively, which are predominantly attributed to the organic components derived from collagen, C–N bond represented to the amide and C–F bond may also be ascribed to the chemical bonding between organic and inorganic compounds.

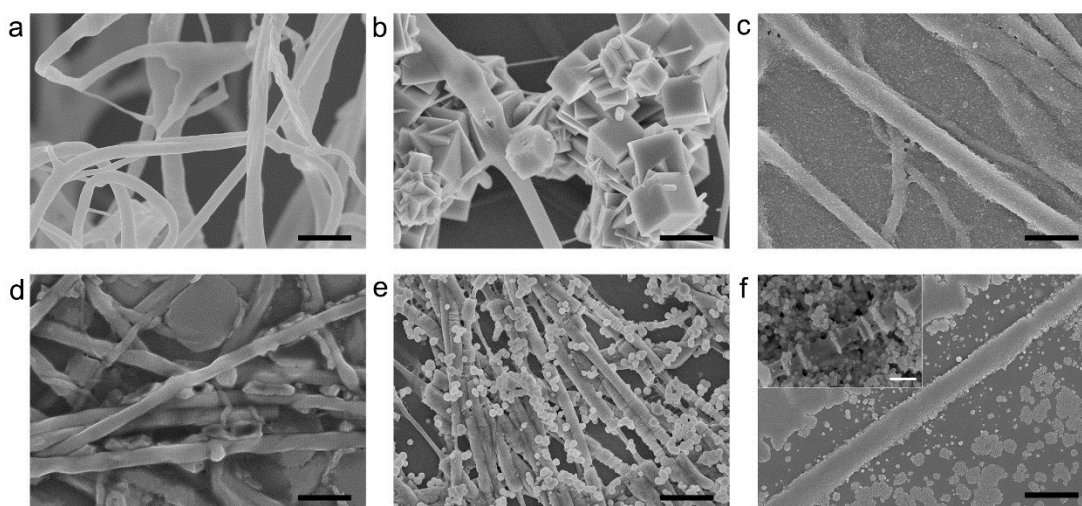


Figure S4. Mineralized products under different reaction conditions. (a) Original collagen fibrils, (b) without PAA, (c) with PAA of 400 $\mu\text{g/ml}$, (d) low content of Ca^{2+} and F^- (2.5 mM) with PAA of 200 $\mu\text{g/ml}$, (e) high content of Ca^{2+} and F^- (10 mM) with PAA of 200 $\mu\text{g/ml}$. (f) with pAsp of 200 $\mu\text{g/ml}$ (Scale bar in (a-d) and (f), 1 μm ; in (e), 2 μm)

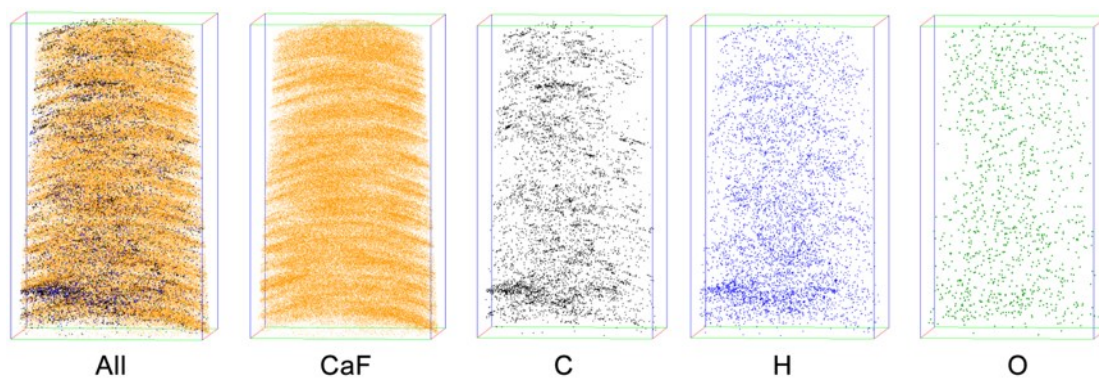


Figure S7. APT reconstruction of CaF_2 mineralized collagen fibrils. The elements distribution of CHO were lower than CaF and the merged tomogram shows that the collagen molecules were uniform distributed within the composite fibril. (X: 46.5 nm, Y: 46.5 nm, Z: 80.4 nm)

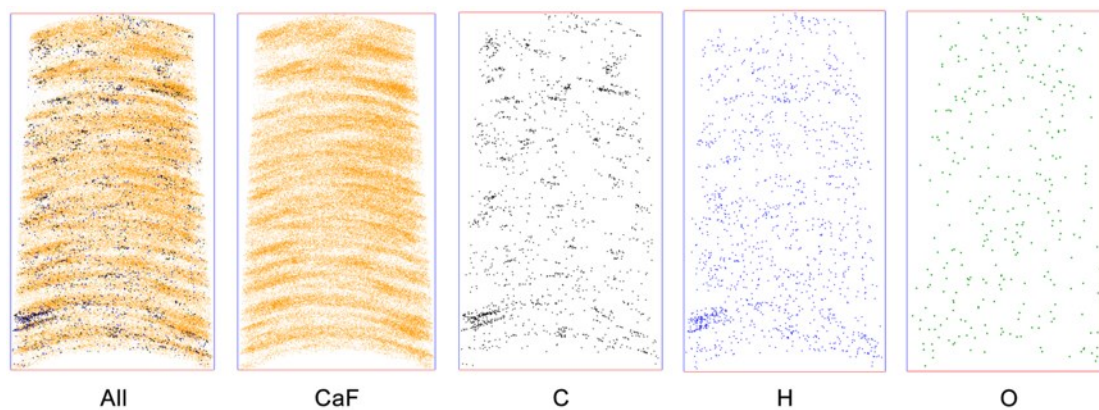


Figure S8. A 8 nm slice from figure S7. (X: 46.5 nm, Y: 8.0 nm, Z: 80.4 nm)

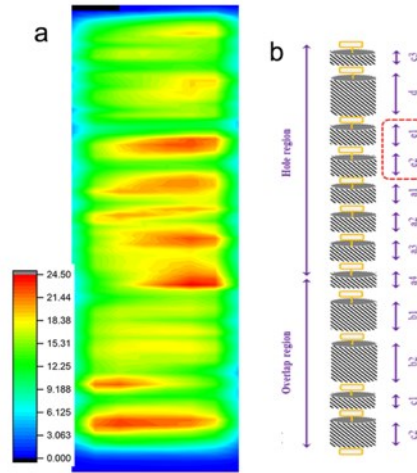


Figure S9. Comparison of CaF atomic density in mineralized collagen (a) and the substructure of collagen fibril in one period (b). Figure b was cited from ref. 17.

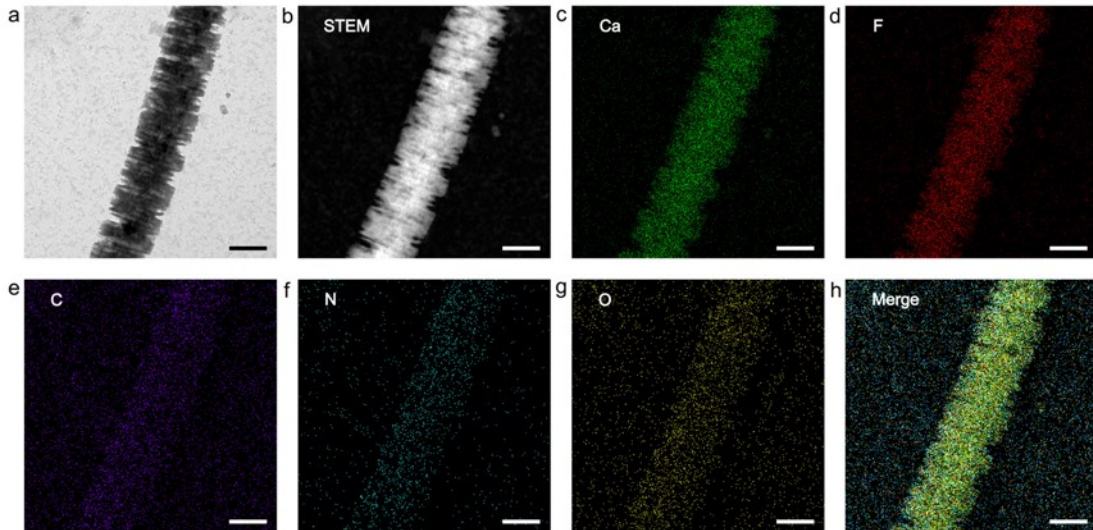


Figure S10. Energy dispersive spectroscopy (EDS) mapping of mineralized collagen fibril for 60 min (Scale bar, 500 nm). (a) TEM image; (b) STEM image; (c-g) Ca, F, C, N and O elements, (h) Merge image.

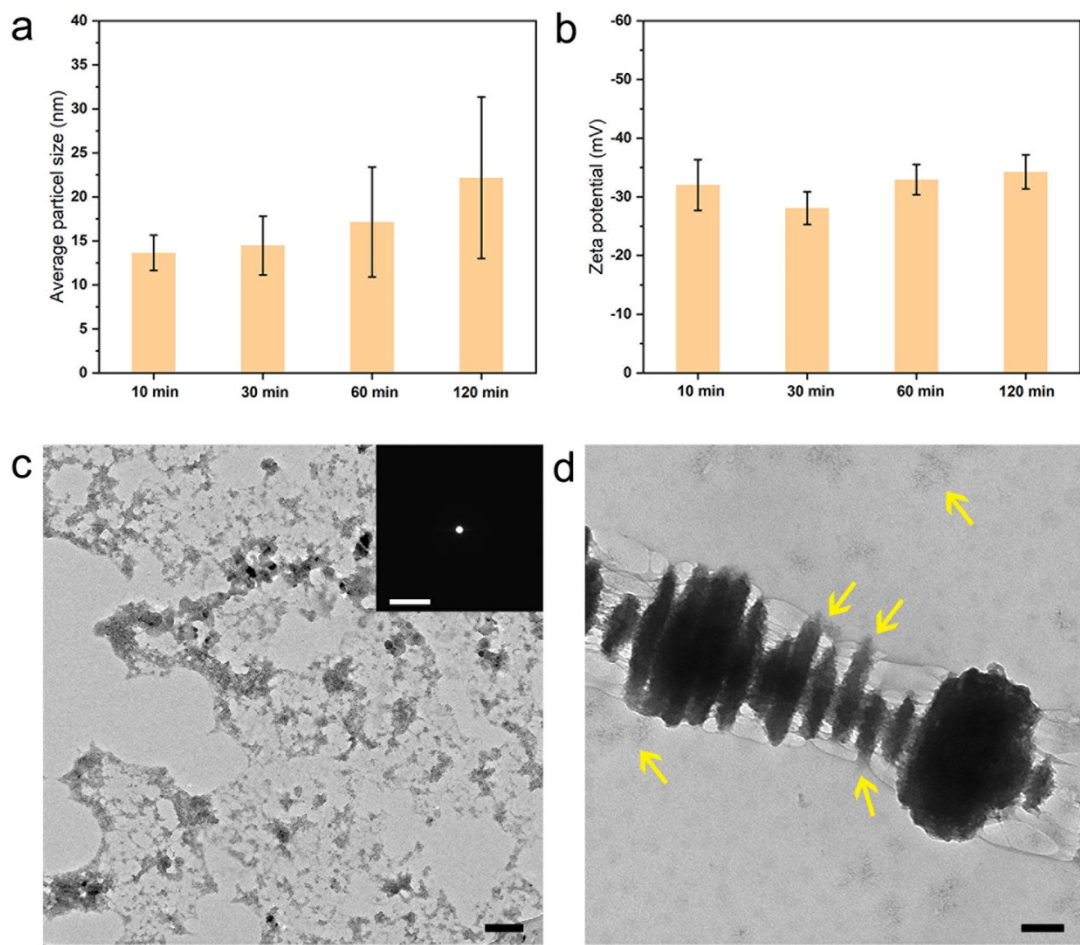


Figure S11. (a) DLS and (b) zeta potential of amorphous CaF₂. (c) TEM image of amorphous CaF₂ after 120 min (Scale bar in TEM, 200 nm; in SAED, 2 1/nm). (d) TEM image of mineralized collagen fibril for 30 min (Scale bar, 100 nm).

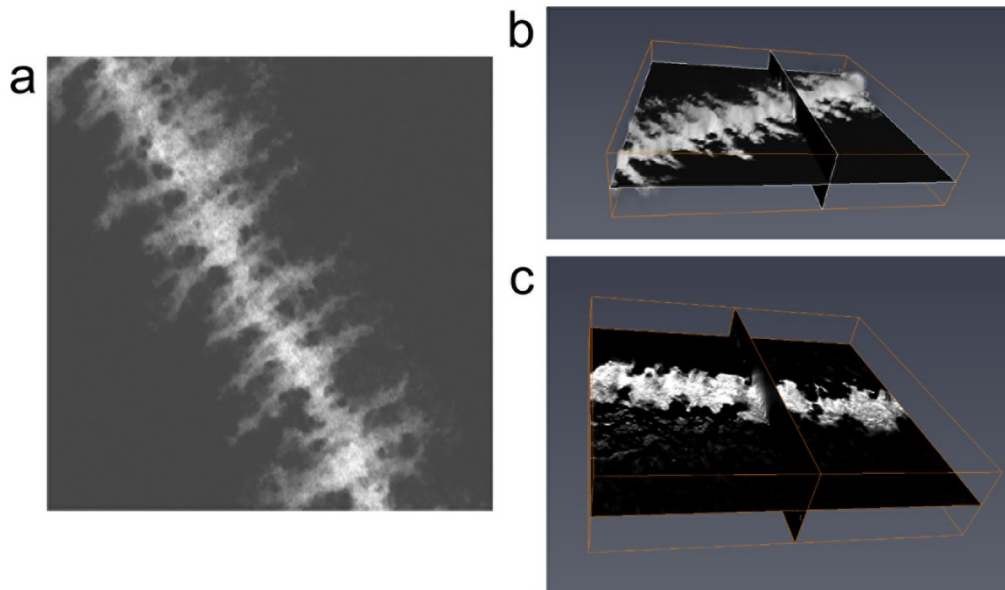


Figure S12. TEM 3D tomography of mineralized collagen fibril. (a) Slice from a section of the three-dimensional volume along the xy plane from (b), (b) segmentation of the computer-generated three-dimensional visualization of 30 min mineralized collagen fibril, (c) segmentation of the computer-generated three-dimensional visualization of 60 min mineralized collagen fibril.

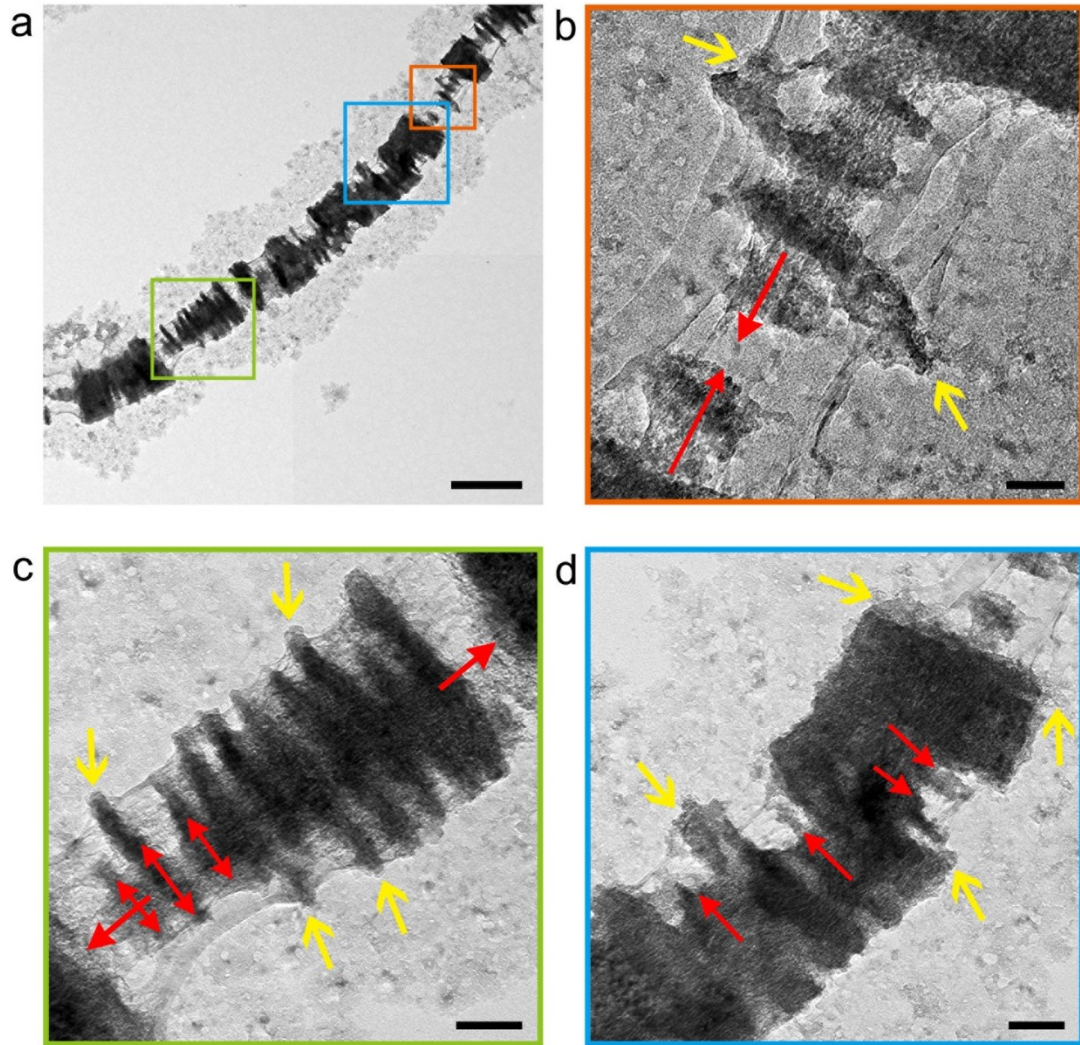


Figure S13. Growth routes in mineralized collagen fibril for 60 min. (a) TEM image of an isolated mineralized collagen fibril. (b-d) The high magnification TEM images in (a), border marked by different color. (b) orange, (c) green, (d) blue. The infiltration of ACF was marked by yellow arrows, the growth direction of minerals was marked by red arrows. (Scale bar in (a), 500 nm; in (b), 50 nm; in (c) and (d), 100 nm)
 ACF infiltrates into the gap zones and transforms to crystalline phase, then spreads along the center axis, finally fills the overlap zone to fully mineralized collagen fibril.

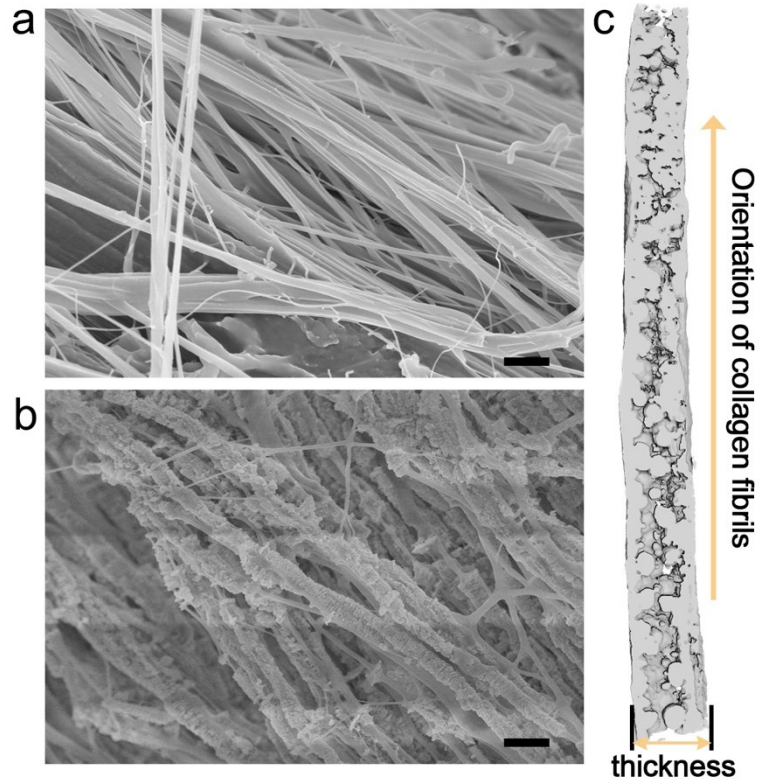


Figure S14. Structure information of mineralized tendon slice. (a) SEM image of original tendon on surface (Scale bar, 1 μm), (b) SEM image of mineralized tendon on surface (Scale bar, 1 μm), (c) Micro-CT image of mineralized tendon (XZ-plane).

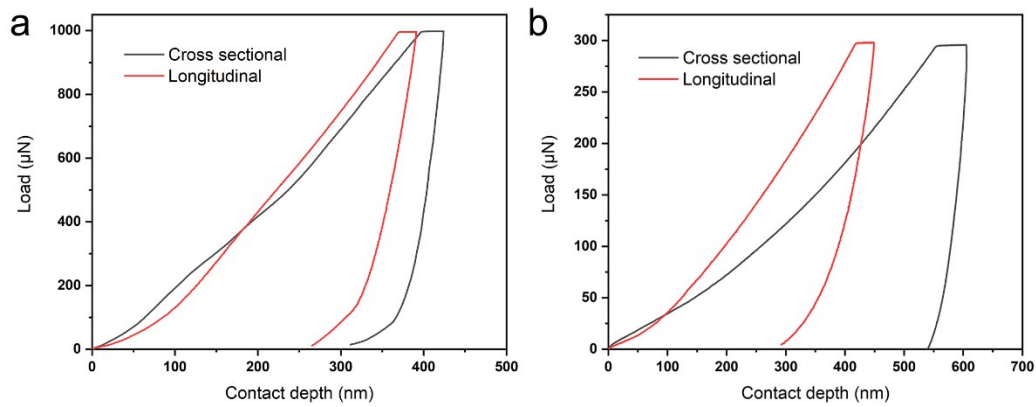


Figure S15. Loading-unloading curves extracted from nanoindentation studies on different sections of (a) mineralized tendon and (b) original tendon.

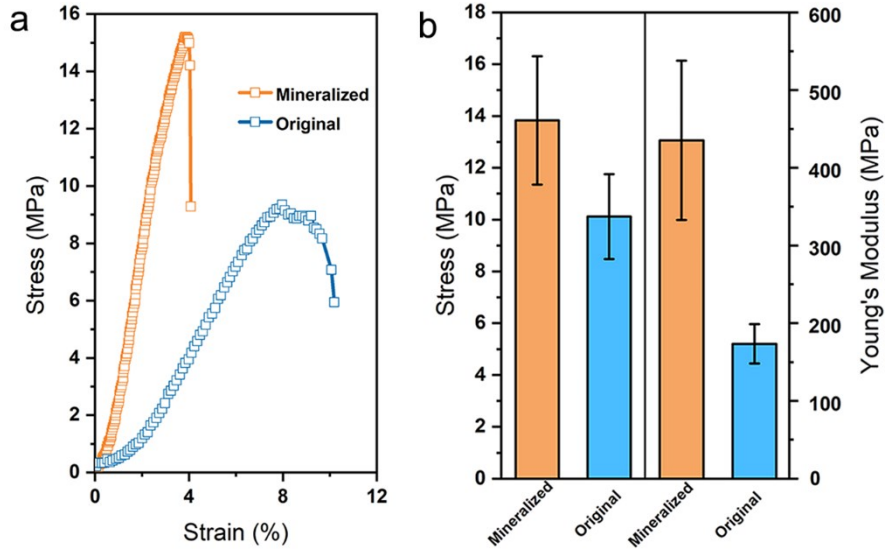


Figure S16. (a) Stress-strain curves of original and mineralized tendons. (b) Tensile strength and elastic modulus of original and mineralized tendons in water.

Table S1 Mechanical properties of the reported collagen based composites using various testing methods.

Collagen composites	Inorganic components	Testing methods	Mechanical properties	Refs.
Collagen sponges	silica	Compressive	Elastic modulus 599.8±166 kPa (dry) Toughness 165.3±5 kPa (dry)	1
Dense collagen gels	HAP	Compressive	Modulus 349±38 kPa (hydrated)	2
Collagen Scaffolds	Silica/HAP	Compressive	Modulus 1.0 MPa (dry) Stress <0.1 MPa (dry)	3
Collagen sponges	HAP	Compressive	Young's modulus 487.5±78.1 kPa (dry)	4
Collagen gel strip	Carbonated HAP	Tensile	Strength ~1.4 MPa (dry) Apparent modulus ~4.7 MPa (dry)	5
Dense collagen scaffolds	HAP	Tensile	Modulus 1.0 MPa (dry) Stress <0.1 MPa (dry)	6
Single collagen fibrils	Nanocarbonate d apatite	Nanomechanical testing (AFM)	Young's modulus 13.7±2.6 GPa (dry)	7
Collagen 3D Scaffold	HAP	Nanomechanical testing (AFM)	Young's modulus 8.92±1.21 GPa (dry)	8
Collagen sponges	Silica/HAP	NanoDMA	Storage modulus ~7.5 GPa (dry)	9
Densified collagen films	HAP	Nanoindentation	Hardness 0.7±0.1 GPa (dry) Elastic modulus 9.1±1.4 GPa (dry) Hardness 177±31 kPa (hydrated) Elastic modulus 8±3 kPa (hydrated)	10
Self-Assembled	Apatite	Nanoindentation	Modulus 6.49±1.87 GPa (dry)	11

Collagen 3D scaffolds				
Rat tail tendon	Fluoridated apatite	Nanoindentation	Elastic modulus 5.6±2.0 GPa (0.5 ppm F ⁻ , hydrated)	12
CaP-PILP recovered bone	HAP	Nanoindentation	Young's modulus 14.3 GPa (dry) Hardness 371.8 MPa (dry)	13
Remineralized dentin	HAP	Nanoindentation	Young's modulus 18.7 GPa (dry) Hardness 610 MPa (dry)	14
Human dentin	HAP	Nanoindentation	Young's modulus 22 GPa (dry) Hardness 0.7 GPa (dry) Young's modulus ~4 GPa (rehydrated) Hardness 0.1 GPa (rehydrated)	15
Human lamellar bone	HAP	Nanoindentation	Young's modulus 21.2±0.6 GPa (dry) Hardness 0.71±0.01 GPa (dry)	16
Mineralized turkey tendon	CaF ₂	Tensile	Tensile stress 13.8±2.5 MPa (hydrated) Young's modulus 435.3±102.5 MPa (hydrated)	This work
Mineralized turkey tendon	CaF ₂	Nanoindentation	Elastic modulus 25.7±2.4 GPa (dry, cross sectional), 25.1±4.1 GPa (dry, longitudinal) Hardness 1.2±0.3 GPa (dry, cross sectional), 1.5±0.5 GPa (dry, longitudinal)	This work

References:

1. Y. Li, T. T. Thula, S. Jee, S. L. Perkins, C. Aparicio, E. P. Douglas, L. B. Gower, Biomimetic Mineralization of Woven Bone-Like Nanocomposites: Role of Collagen Cross-Links. *Biomacromolecules* **2012**, 13, 49-59.
2. L.-N. Niu, K. Jiao, Y.-P. Qi, C. K. Y. Yiu, H. Ryou, D. D. Arola, J.-H. Chen, L. Breschi, D. H. Pashley, F. R. Tay, Infiltration of Silica Inside Fibrillar Collagen. *Angew. Chem. Int. Ed.* **2011**, 50, 11688-11691.
3. L.-N. Niu, K. Jiao, H. Ryou, C. K. Y. Yiu, J.-H. Chen, L. Breschi, D. D. Arola, D. H. Pashley, F. R. Tay, Multiphase Intrafibrillar Mineralization of Collagen. *Angew. Chem. Int. Ed.* **2013**, 52, 5762-5766.
4. B. Marelli, C. E. Ghezzi, A. Alessandrino, J. E. Barralet, G. Freddi, S. N. Nazhat, Silk fibroin derived polypeptide-induced biomineralization of collagen. *Biomaterials* **2012**, 33, 102-108.
5. N. Nassif, F. d. r. Gobeaux, J. Seto, E. Belamie, P. Davidson, P. Panine, G. Mosser, P. Fratzl, M.-M. Giraud Guille, Self-Assembled Collagen–Apatite Matrix with Bone-like Hierarchy. *Chem. Mater.* **2010**, 22, 3307-3309.
6. N. Saxena, M. A. Cremer, E. S. Dolling, H. Nurrohman, S. Habelitz, G. W. Marshall, L. B. Gower, Influence of fluoride on the mineralization of collagen via the polymer-induced liquid-

- precursor (PILP) process. *Dent. Mater.* **2018**, 34, 1378-1390.
7. B. Marelli, C. E. Ghezzi, J. E. Barralet, S. N. Nazhat, Collagen gel fibrillar density dictates the extent of mineralization in vitro. *Soft Matter* **2011**, 7, 9898-9907.
 8. B. Marelli, C. E. Ghezzi, J. E. Barralet, A. R. Boccaccini, S. N. Nazhat, Three-Dimensional Mineralization of Dense Nanofibrillar Collagen–Bioglass Hybrid Scaffolds. *Biomacromolecules* **2010**, 11, 1470-1479.
 9. S. Heinemann, C. Heinemann, M. Jäger, J. Neunzehn, H. P. Wiesmann, T. Hanke, Effect of Silica and Hydroxyapatite Mineralization on the Mechanical Properties and the Biocompatibility of Nanocomposite Collagen Scaffolds. *ACS Appl. Mater. Interfaces* **2011**, 3, 4323-4331.
 10. Y. Liu, D. Luo, X.-X. Kou, X.-D. Wang, F. R. Tay, Y.-L. Sha, Y.-H. Gan, Y.-H. Zhou, Hierarchical Intrafibrillar Nanocarbonated Apatite Assembly Improves the Nanomechanics and Cytocompatibility of Mineralized Collagen. *Adv. Funct. Mater.* **2013**, 23, 1404-1411.
 11. Y. Liu, S. Liu, D. Luo, Z. Xue, X. Yang, L. Gu, Y. Zhou, T. Wang, Hierarchically Staggered Nanostructure of Mineralized Collagen as a Bone-Grafting Scaffold. *Adv. Mater.* **2016**, 28, 8740-8748.
 12. Q. Song, K. Jiao, L. Tonggu, L. G. Wang, S. L. Zhang, Y. D. Yang, L. Zhang, J. H. Bian, D. X. Hao, C. Y. Wang, Y. X. Ma, D. D. Arola, L. Breschi, J. H. Chen, F. R. Tay, L. N. Niu, Contribution of biomimetic collagen-ligand interaction to intrafibrillar mineralization. *Sci. Adv.* **2019**, 5, eaav9075.
 13. S. Yao, X. Lin, Y. Xu, Y. Chen, P. Qiu, C. Shao, B. Jin, Z. Mu, N. A. J. M. Sommerdijk, R. Tang, Osteoporotic Bone Recovery by a Highly Bone-Inductive Calcium Phosphate Polymer-Induced Liquid-Precursor. *Adv. Sci.* **2019**, 6, 1900683.
 14. Y. Qu, T. Gu, Q. Du, C. Shao, J. Wang, B. Jin, W. Kong, J. Sun, C. Chen, H. Pan, R. Tang, X. Gu, Polydopamine Promotes Dentin Remineralization via Interfacial Control. *ACS Biomater. Sci. Eng.* **2020**, 6, 3327-3334.
 15. Y. Qi, Z. Cheng, Z. Ye, H. Zhu, C. Aparicio, Bioinspired Mineralization with Hydroxyapatite and Hierarchical Naturally Aligned Nanofibrillar Cellulose. *ACS Appl. Mater. Interfaces* **2019**, 11, 27598-27604.
 16. T. Tang, W. Wagermaier, R. Schuetz, Q. Wang, F. Eltit, P. Fratzl, R. Wang, Hypermineralization in the femoral neck of the elderly. *Acta Biomater.* **2019**, 89, 330-342.